

# Computation of brittle fracture propagation in strain gradient materials by the FEniCS library

Mathematics and Mechanics of Solids  
2021, Vol. 26(3) 325–334

© The Author(s) 2020

Article reuse guidelines:

[sagepub.com/journals-permissions](https://sagepub.com/journals-permissions)

DOI: 10.1177/1081286520954513

[journals.sagepub.com/home/mms](https://journals.sagepub.com/home/mms)



**E Barchiesi**

*Università degli Studi dell'Aquila, L'Aquila, Italy*

**H Yang**

*Technische Universität Berlin, Berlin, Germany*

**CA Tran**

*Università degli Studi dell'Aquila, L'Aquila, Italy*

**L Placidi**

*International Telematic University Uninettuno, Rome, Italy*

**WH Müller**

*Technische Universität Berlin, Berlin, Germany*

Received 27 April 2020; accepted 11 August 2020

## Abstract

Strain gradient continuum damage modelling has been applied to quasistatic brittle fracture within an approach based on a maximum energy-release rate principle. The model was implemented numerically, making use of the FEniCS open-source library. The considered model introduces non-locality by taking into account the strain gradient in the deformation energy. This allows for stable computations of crack propagation in differently notched samples. The model can take wedges into account, so that fracture onset can occur at wedges. Owing to the absence of a damage gradient term in the dissipated energy, the normal part of the damage gradient is not constrained on boundaries. Thus, non-orthogonal and non-parallel intersections between cracks and boundaries can be observed.

## Keywords

Strain gradient elasticity, brittle fracture, FEniCS, variational principles, regularization

## 1. Introduction

Continuum mechanics has been widely used to study damage phenomena [1–13]. In continuum damage models, the studied system is described not only by a displacement field, but also by a damage field. Thus, there is one

---

### Corresponding author:

H Yang, Technische Universität Berlin, Berlin, Germany.

Email: [hua.yang@campus.tu-berlin.de](mailto:hua.yang@campus.tu-berlin.de)

more independent variable when compared with the usual elasticity models. In this work, such a damage field is considered, to take the local deterioration of the material into account. Furthermore, healing mechanisms are not considered, so that damage is assumed to be non-decreasing in time.

### *1.1. Localization phenomena in damage mechanics*

Continuum damage models usually involve localization phenomena [14–17]: the stress and the strain concentrate in small regions. This phenomenon must be taken into account by the numerical model to avoid instability or mesh-dependence. The size of such regions of concentration can be considered as a length scale characterizing the studied material. As such, it must also be acknowledged by the mathematical model. This is the aim of non-local damage models: the length scale is introduced in order to control how much the deformation varies in space. In a variational framework, this means regularizing the solution by penalizing the candidate displacements that are too localized.

For example, in damage gradient models, the elastic strain energy depends on the gradient of the damage field, allowing one to deal with localization and mesh-dependence. In this work, the non-locality is based on the dependence of the deformation energy on strain gradient instead of damage gradient [4].

Damage may also be considered as a microstructure having macroscopic effects. Materials showing such structures have at least been known since the nineteenth century [18–21] and were widely studied during the last decades [22–28]. In particular, strain gradient models have been extensively applied to microstructured materials [29–40].

### *1.2. Maximum energy-release principle to model damaging phenomena*

In this work, the mathematical problem to be solved is derived from the maximum energy-release principle, which is a variational inequality [41, 42] aimed at modelling dissipative systems, and generalizing the least action principle. Using a variational approach has many advantages [43], one being that it is possible to derive the boundary conditions, ensuring well-posedness of the problem [44, 45]. Furthermore, the weak form can be simply recovered [46–51], this being convenient if the problem is solved using a numerical method based on weak forms, such as finite-element methods [52–70]. The maximum energy-release principle used in this work requires the specification of the energy released in damaging [4, 71, 72].

### *1.3. Strain gradient damage model for quasistatic brittle fracture*

The model studied in this work considers an isotropic two-dimensional continuum, showing geometrically non-linear elastic behaviour, and undergoing quasistatic brittle fracture. The kinematic description relies on a displacement and a damage field, where the latter is assumed to be non-decreasing in time. The application of the maximum energy-release principle yields both balance equations and Karush–Kuhn–Tucker conditions. The considered energy terms include a dissipated energy depending on damage (but not on its gradient), and a deformation energy depending on both strain and strain gradient. Moreover, the deformation energy involves elastic coefficients, which are assumed to depend on the local damage.

### *1.4. Plan of the work*

The paper is structured as follows. In Section 2, the mathematical model is presented. The frameworks of elasticity and damage are introduced, followed by the variational derivation of the problem to be solved. The numerical model is then presented in Section 3 by explaining the solution algorithm and the software implementation. Numerical results are given in Section 4 for two applications on notched samples. Finally, Section 5 presents concluding remarks.

## **2. Strain gradient modelling of brittle fracture**

The reference configuration of the studied two-dimensional body is represented by an open set  $\Omega \subset \mathbb{R}^2$  and its boundary  $\partial\Omega$ . A Cartesian coordinate system  $(O, (e_1, e_2))$  is defined, in which any generic point  $X \in \Omega$  has the coordinates  $(X_1, X_2)$ .

Using a Lagrangian framework, the kinematics of the model, as well as the different energy quantities that are used to derive the equations of the problem from the maximum energy-release principle, will be defined in this section.

## 2.1. Elasticity framework

The modelling of an undamaged elastic body is described first. Damage effects are left to Subsection 2.2.

**2.1.1. Kinematics – first independent variable.** The placement  $\chi : \Omega \rightarrow \mathbb{R}^2$  is defined to be the map that relates to any point  $X \in \Omega$  to its current position  $\chi(X)$ . Thus,  $\chi(\Omega)$  is the current configuration. The displacement is then defined as  $u(X) = \chi(X) - X$ . It is the first independent variable of the problem.

At this point, the gradient of placement  $F = \nabla \chi$  with respect to the space variable in the reference configuration, as well as the gradient of displacement  $\nabla u = F - I$ , shall be introduced.<sup>1</sup> The local deformation of the body is described by the Green–Lagrange strain tensor  $G = (F^T F - I)/2$ . As in brittle fracture only small zones in the proximity of the crack tip undergo large deformations, the so-called small strain hypothesis is generally accepted, where quadratic terms in  $\nabla u$  are neglected, i.e.  $G = \epsilon = (\nabla u + \nabla u^T)/2$ . Henceforth, we will make use of such an assumption.

**2.1.2. Strain gradient internal energy.** The studied system is assumed to be isotropically elastic. Its deformation energy (when undamaged, i.e. its recoverable elastic energy)  $W_{\text{def}}$  is defined as the integration in space of a quadratic form of the strain and its gradient:

$$W_{\text{def}} = \int_{\Omega} \left( \frac{1}{2} \epsilon_{ij} C_{ijkl} \epsilon_{kl} + \frac{1}{2} \epsilon_{ij,k} D_{ijklmn} \epsilon_{lm,n} \right) dA \quad (1)$$

with

$$\begin{aligned} C_{ijkl} &= c_1 \delta_{ij} \delta_{kl} + c_2 (\delta_{ik} \delta_{jl} + \delta_{il} \delta_{jk}), \\ D_{ijklmn} &= c_3 (\delta_{ij} \delta_{kl} \delta_{mn} + \delta_{in} \delta_{jk} \delta_{lm} + \delta_{ij} \delta_{km} \delta_{ln} + \delta_{ik} \delta_{jn} \delta_{lm}) + c_4 \delta_{ij} \delta_{kn} \delta_{ml} \\ &\quad + c_5 (\delta_{ik} \delta_{jl} \delta_{mn} + \delta_{im} \delta_{jk} \delta_{ln} + \delta_{ik} \delta_{jm} \delta_{ln} + \delta_{il} \delta_{jk} \delta_{mn}) + c_6 (\delta_{il} \delta_{jm} \delta_{kn} + \delta_{im} \delta_{jl} \delta_{kn}) \\ &\quad + c_7 (\delta_{il} \delta_{jn} \delta_{mk} + \delta_{im} \delta_{jn} \delta_{lk} + \delta_{in} \delta_{jl} \delta_{km} + \delta_{in} \delta_{jm} \delta_{kl}). \end{aligned} \quad (2)$$

Note that, when dealing with 2D isotropic materials, there are only four independent parameters out of the five parameters  $c_3, c_4, c_5, c_6, c_7$  in  $D_{ijklmn}$ , see a discussion in [73]. The first-gradient coefficients (Lamé coefficients) can be expressed by the Young modulus  $E$  and Poisson ratio  $\nu$ :

$$c_1 = \frac{E\nu}{(1+\nu)(1-2\nu)}, \quad c_2 = \frac{E}{2(1+\nu)}. \quad (3)$$

**2.1.3. Exterior work.** The considered external effects are modelled as the works of a bulk force  $b$ , a bulk double force  $m$  per unit area, a contact force  $t$  and a contact double force  $s$  per unit length:

$$W_{\text{ext}} = \int_{\Omega} (b_i u_i + m_{ij} u_{i,j}) dA + \int_{\partial\Omega} (t_i u_i + s_{ij} u_{i,j}) dl \quad (4)$$

## 2.2. Damage modelling

It will now be shown how damage is taken into account in both the deformation and dissipation occurring in the system. More details about the chosen model can be found in [4].

**2.2.1. Kinematics – second independent variable.** Damage is modelled as a scalar field  $\omega : \Omega \rightarrow [0, 1]$ , which is the second independent variable of the problem. Although the elastic model takes into account both the first and second gradients of deformation, we assume in this work that there is only one damage field, instead of

considering one damage field acting on first-gradient deformation mechanisms and another field for the second gradient. This assumption is made first for simplification, and shall be investigated in future works.

For every  $X \in \Omega$ ,  $\omega(X)$  represents the local damage state of the particle that was at point  $X$  in the reference configuration. The damage values go from 0, for a non-damaged material, to 1, for a totally damaged material. Since no healing mechanism is considered, the damage field is assumed to be non-decreasing in time.

**2.2.2. Apparent stiffness loss and energy dissipation.** The damage field has two effects on the energy of the system. First, every damaged area undergoes an apparent loss of stiffness. This phenomenon is taken into account by assuming that the stiffness coefficients  $C_{ijkl}$  and  $D_{ijklmn}$  depend on the local damage. Thus, the deformation energy depends not only on the strain and strain gradient, but also on the damage field. Second, the energy lost in damaging phenomena is also taken into account as a dissipation term  $W_{\text{diss}}$ , which is added to the deformation energy as part of the internal energy  $W_{\text{int}} = W_{\text{def}} + W_{\text{diss}}$ .

**Deformation energy for the damaged material.** As stated, the effectiveness of the stiffness coefficients  $C_{ijkl}$  and  $D_{ijklmn}$  must correlate with the damage field  $\omega$ . Two parameters,  $n, m \in ]-\infty, 1]$ , are introduced for this purpose, as follows:

$$W_{\text{int}} = \int_{\Omega} \left( (1 - m\omega) \frac{1}{2} \epsilon_{ij} C_{ijkl} \epsilon_{kl} + (1 - n\omega) \frac{1}{2} \epsilon_{ij,k} D_{ijklmn} \epsilon_{lm,n} \right) dA. \quad (5)$$

The  $n$  and  $m$  parameters allow one to model the behaviour of the damaged material. More specifically:

- If  $n, m > 0$ , then the more damaged the material is, the more its stiffness decreases locally. For the limit value  $n = 1$  or  $m = 1$ , the corresponding stiffness vanishes when the material is locally totally damaged.
- If  $n, m < 0$ , then an increasing damage also increases the local stiffness. This may happen, for example, when the damage changes the microstructure of the material, resulting in an effective stiffening.

One should note that the problem is no longer well-posed for the limit value  $n = 1$  or  $m = 1$ , since the corresponding stiffnesses vanish. It is thus preferable to stop at a lower value, for example,  $n = 0.999$  and  $m = 0.999$ .

**Dissipated energy.** The dissipated energy is modelled by a functional  $W_{\text{diss}}$ . It involves two parameters  $K_1, K_2 \in \mathbb{R}_+$ . The former represents a threshold ruling the appearance and increase of damage, while the latter models the resistance of the material to damaging phenomena:

$$W_{\text{diss}} = \int_{\Omega} \left( K_1 \omega + \frac{1}{2} K_2 \omega^2 \right) dA. \quad (6)$$

It is added to the internal energy  $W_{\text{int}}$ , along with the deformation term:

$$\begin{aligned} W_{\text{int}} &= W_{\text{def}} + W_{\text{diss}} \\ &= \int_{\Omega} \left( (1 - m\omega) \frac{1}{2} \epsilon_{ij} C_{ijkl} \epsilon_{kl} + (1 - n\omega) \frac{1}{2} \epsilon_{ij,k} D_{ijklmn} \epsilon_{lm,n} \right) dA + \int_{\Omega} \left( K_1 \omega + \frac{1}{2} K_2 \omega^2 \right) dA. \end{aligned} \quad (7)$$

### 2.3. Discrete-time maximum energy-release principle

So far, the model has been presented by considering a reference configuration  $\Omega$  and one current configuration  $\chi(\Omega)$ . The load parameter  $\lambda \in \mathbb{R}$  shall now be introduced, so that one may consider a sequence of configurations  $\chi^\lambda(\Omega)$ .

**2.3.1. Potential energy.** At this point, the total potential energy  $\mathcal{E}^\lambda$  associated to the configuration  $\chi^\lambda(\Omega)$  of the system, defined for every admissible motion  $\hat{u}$  and non-decreasing admissible damage  $\hat{\omega}$ , is introduced as:

$$\begin{aligned} \mathcal{E}^\lambda(\hat{u}, \hat{\omega}) &= W_{\text{int}}^\lambda(\hat{\epsilon}_{ij}, \hat{\epsilon}_{ij,k}, \hat{\omega}) - W_{\text{ext}}^\lambda(\hat{u}, \nabla \hat{u}) \\ &= W_{\text{def}}^\lambda(\hat{\epsilon}_{ij}, \hat{\epsilon}_{ij,k}, \hat{\omega}) + W_{\text{diss}}^\lambda(\hat{\omega}) - W_{\text{ext}}^\lambda(\hat{u}, \nabla \hat{u}). \end{aligned} \quad (8)$$

Under the hypothesis of a quasistatic evolution, the kinetic energy is negligible with respect to that potential energy. By applying the maximum energy-release principle, similarly to [4], every solution  $(u^\lambda, \omega^\lambda)$  has to satisfy<sup>2</sup>

$$\delta \mathcal{E}^\lambda(u^\lambda, \omega^\lambda)(\Delta u^\lambda, \Delta \omega^\lambda) \geq \delta \mathcal{E}^\lambda(u^\lambda, \omega^\lambda)(\delta u, \delta \omega) \quad (9)$$

for all admissible displacement and damage variations,  $\delta u$  and  $\delta \omega \geq 0$ , respectively, with  $\Delta u^\lambda = u^\lambda - u^{\lambda-\Delta\lambda}$  and  $\Delta \omega^\lambda = \omega^\lambda - \omega^{\lambda-\Delta\lambda} \geq 0$ ,  $\Delta\lambda \rightarrow 0$  being the step between  $\lambda$  and the previous load parameter.

**2.3.2. Equilibrium for a fixed damage field.** For a null damage variation  $\delta \omega = 0$ , equation (9) yields the stationarity condition usually met for undamaged elastic behaviour,

$$\delta \mathcal{E}^\lambda(u^\lambda, \omega^\lambda)(\delta u, 0) = 0. \quad (10)$$

This is on simplifying the notation,

$$\delta W_{\text{int}} - \delta W_{\text{ext}} = 0, \quad (11)$$

where the variation of internal energy reads

$$\delta W_{\text{int}} = \frac{\partial W_{\text{int}}}{\partial \epsilon_{ij}} \delta \epsilon_{ij} + \frac{\partial W_{\text{int}}}{\partial \epsilon_{ij,k}} \delta \epsilon_{ij,k} + \frac{\partial W_{\text{int}}}{\partial \omega} \delta \omega. \quad (12)$$

Hence, the stationarity condition can be rewritten as

$$\frac{\partial W_{\text{int}}}{\partial \epsilon_{ij}} \delta \epsilon_{ij} + \frac{\partial W_{\text{int}}}{\partial \epsilon_{ij,k}} \delta \epsilon_{ij,k} - \delta W_{\text{ext}} + \frac{\partial W_{\text{int}}}{\partial \omega} \delta \omega = 0, \quad (13)$$

i.e.,

$$\begin{aligned} & \int_{\Omega} \left( (1 - m\omega) \epsilon_{ij} C_{ijkl} \delta \epsilon_{kl} + (1 - n\omega) \epsilon_{ij,k} D_{ijklmn} \delta \epsilon_{lm,n} \right) dA - \int_{\Omega} (b_i \delta u_i + m_{ij} \delta u_{i,j}) dA \\ & - \int_{\partial\Omega} (t_i \delta u_i + s_{ij} \delta u_{i,j}) dl + \int_{\Omega} \left( -\frac{m}{2} \epsilon_{ij} C_{ijkl} \epsilon_{kl} \delta \omega - \frac{n}{2} \epsilon_{ij,k} D_{ijklmn} \epsilon_{lm,n} \delta \omega + K_1 \delta \omega + K_2 \omega \delta \omega \right) dA = 0. \end{aligned} \quad (14)$$

**2.3.3. Karush–Kuhn–Tucker conditions for a fixed displacement field.** For a null displacement variation,  $\delta u = 0$ , one can derive the Karush–Kuhn–Tucker conditions from equation (9) [4], namely:

$$\left\{ \begin{array}{l} \omega^\lambda = \left( \frac{m}{2} \epsilon_{ij} C_{ijkl} \epsilon_{kl} + \frac{n}{2} \epsilon_{ij,k} D_{ijklmn} \epsilon_{lm,n} - K_1 \right) / K_2, \\ \text{or} \\ \omega^\lambda = \omega^{\lambda-1}. \end{array} \right.$$

### 3. Numerical modelling: alternative minimization algorithm

The model presented previously showed a separation between the elastic behaviour for a fixed damage field, on the one hand, and the evolution of damage for a fixed displacement field, on the other hand. This distinction is exploited to implement the studied model numerically through a version of an alternative minimization algorithm (also presented in [4]). In this algorithm, two minimization problems are solved, one after the other, for each load parameter  $\lambda$ .

- First, while keeping the damage field  $\omega^{\lambda-\Delta\lambda}$  of the previous step, the new displacement field  $u^\lambda$  is computed as the solution of the minimization of the potential energy,

$$\mathcal{E}(u^\lambda, \omega^{\lambda-\Delta\lambda}) = \min \{ \mathcal{E}(\hat{u}, \omega^{\lambda-\Delta\lambda}), \hat{u} \text{ admissible displacement} \}. \quad (15)$$

A standard mixed finite-element method for strain gradient mechanics has been employed [74–77], thus introducing extra independent variables during the discretization of the weak form. The extra independent variables were constrained using Lagrange multipliers.

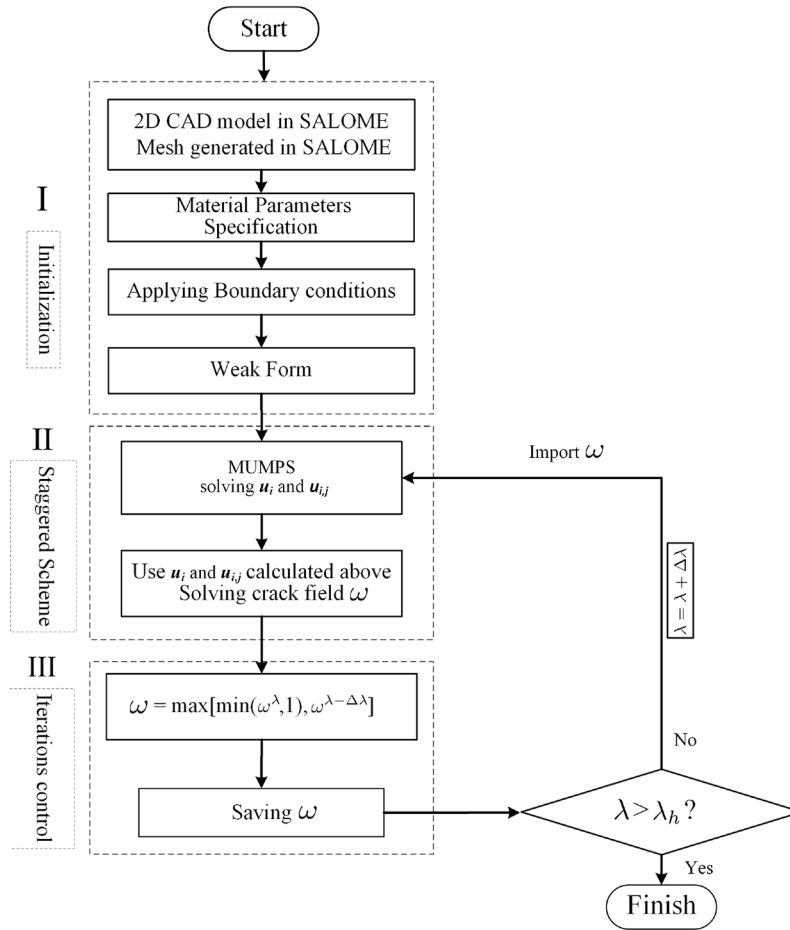


**Figure 1.** Flowchart for the numerical implementation. Here, the load parameter is denoted by  $\lambda$ . The quantity  $\lambda_h$  denotes the time horizon.

- Second, the new damage field  $\omega^\lambda$  is computed by checking the Karush–Kuhn–Tucker conditions with the previously computed displacement field  $u^\lambda$ ,

$$\omega^\lambda = \max \left[ \min \left( \bar{\omega}(u^\lambda), 1 \right), \omega^{\lambda - \Delta\lambda} \right], \quad (16)$$

where  $\bar{\omega}(u^\lambda)$  is the damage threshold value,

$$\bar{\omega}(u^\lambda) = \left( \frac{m}{2} \epsilon_{ij} C_{ijkl} \epsilon_{kl} + \frac{n}{2} \epsilon_{ij,k} D_{ijklmn} \epsilon_{lm,n} - K_1 \right) / K_2. \quad (17)$$

In the undamaged state, this condition means that two events may happen. First, the deformation energy may locally exceed the damage initiation level  $K_1$ , in which case the local damage assumes the (non-zero) difference value divided by  $K_2$ . Second, the damage remains unchanged, thus being equal to zero.

This algorithm is summarized in Figure 1.

#### 4. Numerical results

In what follows, numerical simulations of extension tests for two different samples will be presented. Both samples have initial cracks implemented as an absence of matter (elements), outside of which the material is initially undamaged ( $\omega^0 = 0$ ).

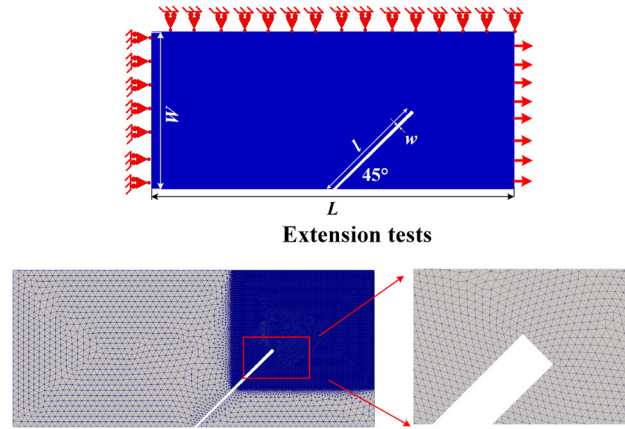


**Figure 2.** Geometry, boundary conditions and mesh for obliquely notched sample.

**Table 1.** Data used for numerical simulations.

Young modulus (GPa)	Poisson ratio	$c_3, c_4, c_5, c_6, c_7$ (N)	$L$ (mm)	$W$ (mm)	$l$ (mm)	$w$ (mm)	$m, n$
75	0.32	I	30	13	10	0.3	0.999

#### 4.1. Case I: oblique notch

**4.1.1. Case I: geometry and numerical data.** The geometry is a rectangle (see Figure 2) of width  $W$  and length  $L$ , in which emerges a straight notch. As one can see in the figure, the notch starts from the middle of the bottom side with a  $45^\circ$  angle, has width  $w$  and length  $l$ .

The boundary conditions are fixed as follows:

- *Left-hand side.* Null horizontal displacement;
- *Top.* Null vertical displacement;
- *Bottom.* Free displacement;
- *Right-hand side.* Imposed displacement (extension).

It shall also be recalled that, in the considered model, it is meaningless to set boundary conditions for damage, since the energy to be minimized does not involve a damage gradient. As a consequence, there is no boundary term involving damage. This may also be seen in the numerical procedure, since the displacement field  $u^\lambda$  is computed by keeping the previous damage  $\omega^{\lambda-\Delta\lambda}$ .

Numerically, the mesh is made of triangular elements. It is finer around the crack, and even more so in the top-right of the sample, where fracture is expected to appear. Table 1 shows the values chosen for the parameters in the simulations. Note that the parameters  $n$  and  $m$  have been chosen in such a way that, when the damage field  $\omega(X)$  is equal to 1, a physically negligible, yet non-zero, amount of elastic energy is still stored at point  $X$  of the continuum. This standard remedy is adopted with the aim of keeping the well-posedness of the elastic problem during crack propagation, as mentioned before.

#### 4.1.2. Case I: results

**Total displacement.** The total displacement is plotted in Figure 3. The propagating crack is visible as a line through which the displacement norm is discontinuous. The last picture shows the final step, when the crack reaches the top side.

**Damage.** The propagation of the crack is more apparent when plotting the damage field (Figure 4). More specifically, two interesting observations can be made:

- The width of the propagating crack is much smaller than the width of the initial notch.

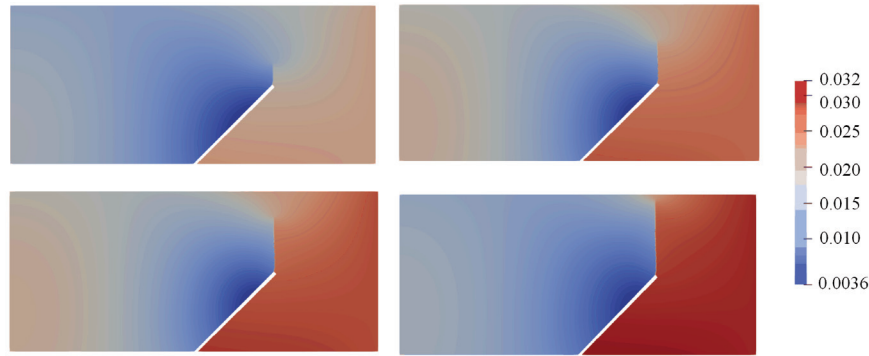


**Figure 3.** Case I – evolution of total displacement.

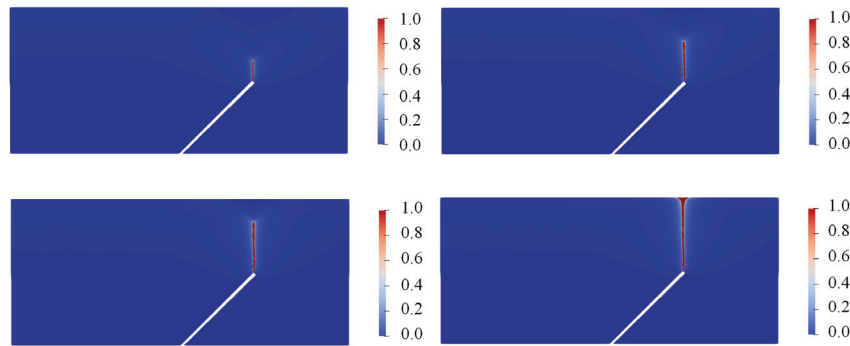


**Figure 4.** Case I – evolution of damage field.

- Consequently, it is clear that the crack appears at a wedge, and that its propagation is not orthogonal to the sides of the notch.

**Stress.** The evolution of the three stress components is plotted in Figure 5. Once again, the propagation of the crack is clearly apparent. Two interesting results are worth noticing:

- Every stress component is zero inside the propagating crack.
- Outside of the crack, the stress is much greater around the propagating crack tip than far from it.

## 4.2. Case 2: notch and hole

**4.2.1. Case 2: geometry and numerical data.** The geometry is again a rectangle (see Figure 6) of width  $W$  and length  $L$ , but the initial cracks are different. Indeed, as can be seen in the figure, there are now:

- A horizontal notch starting from the left-hand side, of length  $l$  and width  $w$ ;
- A hole of diameter 20 mm, whose centre is 28.5 mm from the right-hand side and 51 mm from the bottom.

Concerning the boundary conditions:

- *Bottom.* Null displacement;
- *Lateral sides.* Free displacement;
- *Top.* Imposed displacement (extension).

The mesh visible in Figure 6 is much finer around the initial notches, where cracks are expected to propagate. The numerical values are given in Table 2.



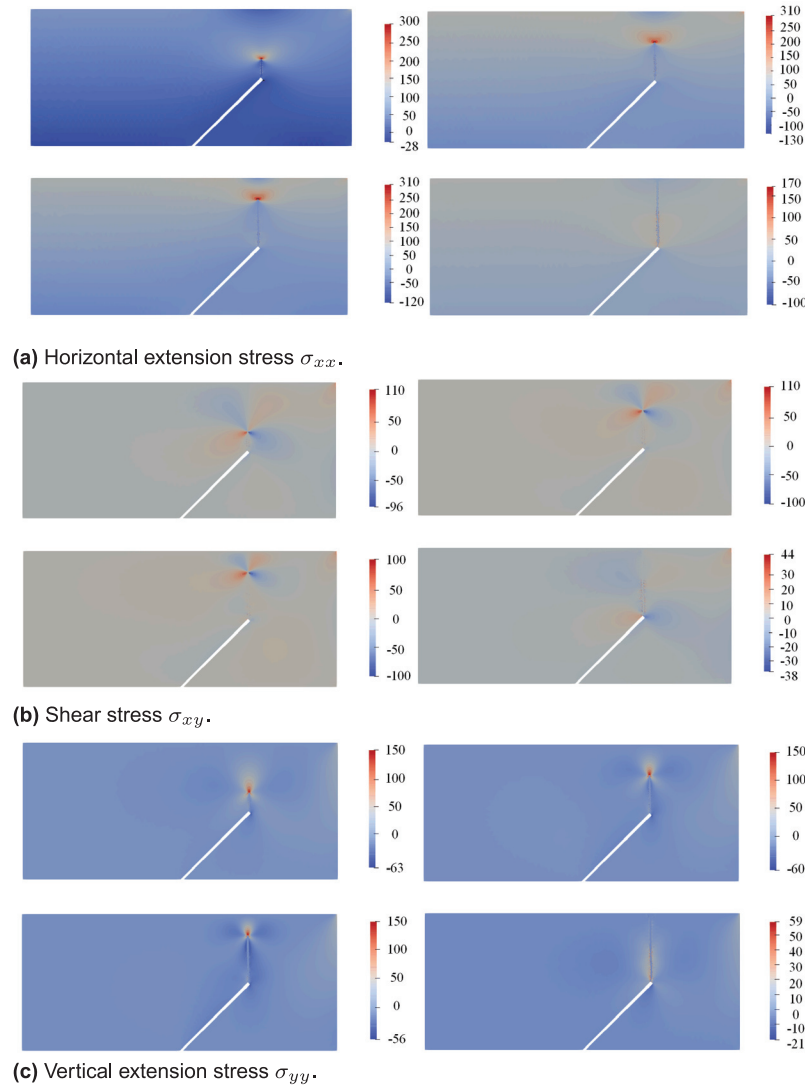


**Figure 5.** Case 1 – evolution of stress components.

**Table 2.** Data used for numerical simulations.

Young modulus (GPa)	Poisson ratio	$c_3, c_4, c_5, c_6, c_7$ (N)	$L$ (mm)	$W$ (mm)	$l$ (mm)	$w$ (mm)	$m, n$
75	0.32	I	120	65	10	I	0.999

#### 4.2.2. Case 2: results

**Damage and total displacement.** The evolution of both damage and displacement fields are plotted in Figure 6, where a crack is propagating from the left-hand side notch towards the central hole. As in Case 1:

- The width of the propagating crack is small enough to see that it starts from a wedge.
- In the final step, the crack clearly reaches the central hole non-orthogonally.

**Stress.** The stress components are plotted in Figure 8. As in the previous case, the stress is concentrated around the propagating crack tip, while being vanishing within the crack.

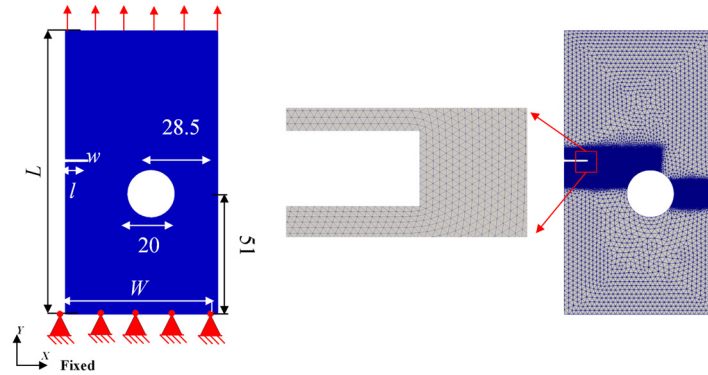


**Figure 6.** Geometry, boundary conditions and mesh for notched sample with hole.

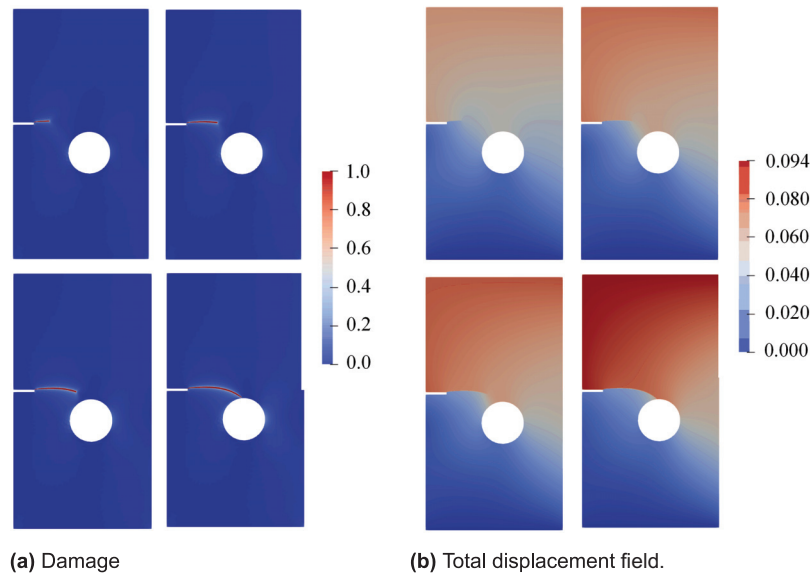


**Figure 7.** Case 2 – evolution of damage and total displacement.

#### 4.3. Interpretation: advantages of the considered model

The numerical results give interesting insight into how damage and stress fields behave in the considered model.

**4.3.1. Stress results.** There were no numerical instabilities, owing to the concentration of stress around the propagating crack: it was always significantly large close to the crack tip, while being vanishing inside the crack itself. This is due to the parameters  $m$  and  $n$  in equation 5, which had values close to 1 in the presented applications (see Tables 1 and 2). The rationale behind this choice is that no elastic energy should be stored within a crack.

**4.3.2. Crack propagation.** The numerical results show that the width of the propagating crack is much smaller than the initial notches. This can be clearly observed in Figure 9. Kinking angles of the cracks departing from the notch tip are, for the first and second tests, approximately  $80^\circ$  and  $25^\circ$ , respectively. A comparison with predictions of the kinking angles made using other means, such as criteria based on stress intensity factors [78, 79], would potentially be beneficial. However, note that these criteria are strictly valid for sharp cracks under external load and not for notches. Thus, they should be compared when the internal phase-field approximation length introduced to approximate the crack is greater than the width of the initial notch, i.e., when fracture onset within the notch is not resolved, as is usually done in damage gradient phase-field theories. A detailed analysis

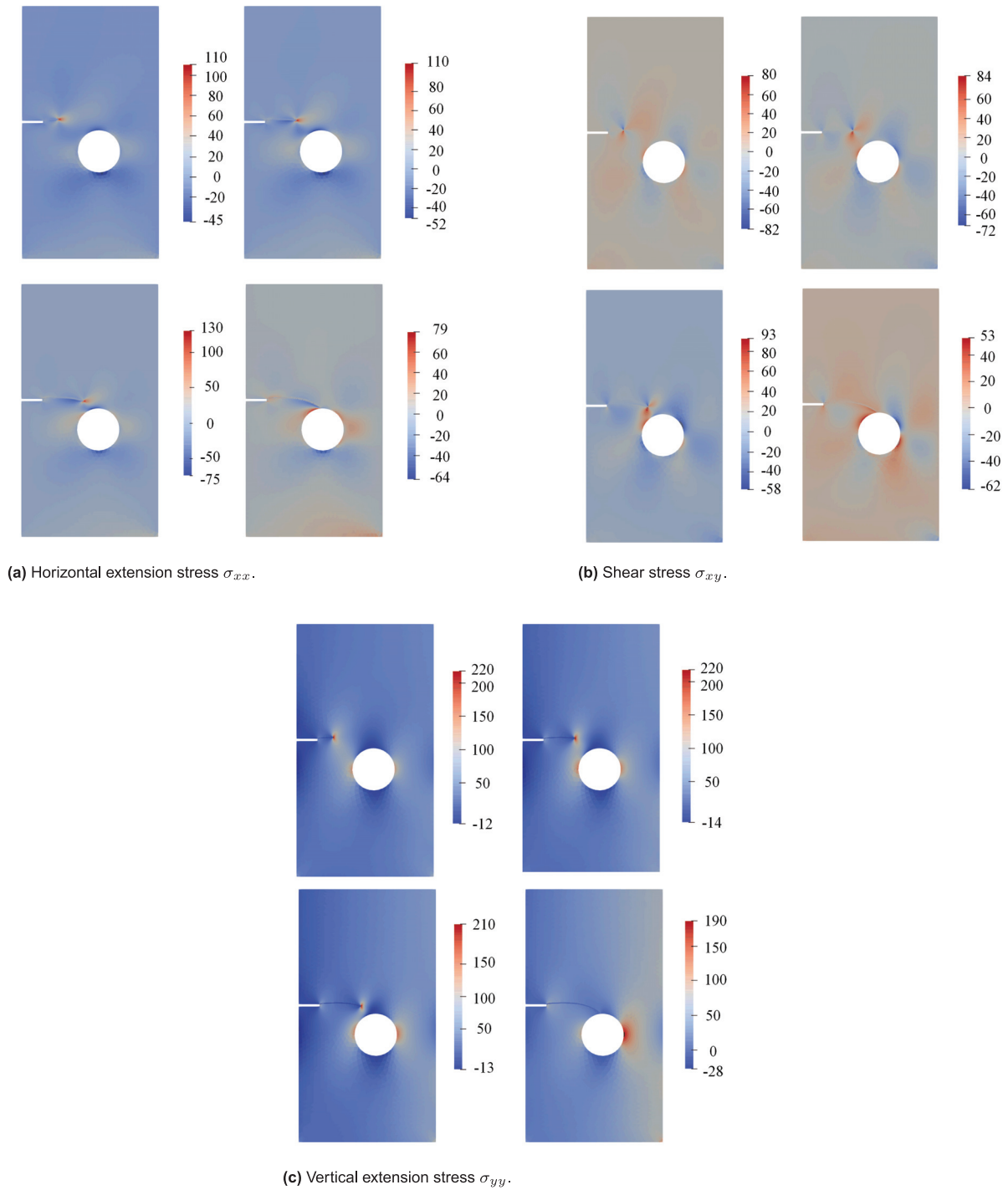


**Figure 8.** Case 2 – evolution of stress components.

is therefore left to future research. However, it is worth remarking here that the dependence of the deformation energy on the strain gradient enables one to go further in the integration by parts when deriving the weak form for the elastic problem, i.e., up to point contributions in the two-dimensional case. Consequently, cracks can start at wedges, which is not possible in damage gradient theories if the second gradient of the damage is not considered [45, 80, 81]. Note that, in damage gradient phase-field theories,<sup>3</sup> essential boundary conditions on the damage field, which are not usually considered as a datum in fracture problems, or natural boundary conditions, enforcing the normal damage gradient to vanish, should be given. The latter condition implies that

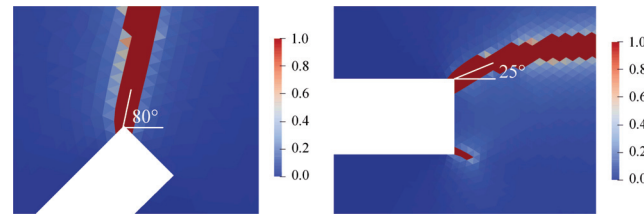


**Figure 9.** A close look at the crack near the notches.

cracks must intersect boundaries either orthogonally or in parallel, which is rather limiting in the description of some real cracking phenomena. When damage gradient theories are applied, the regularization length is chosen to be sufficiently large that the phase-field approximation of the propagating crack can “surround” the initial notch. In this way, there is no more any constraint in terms of, e.g., kinking angle. Clearly, this remedy prevents one from taking into account the effect of the notch tip geometry on the crack propagation. Such an effect could be non-negligible when the ratio between the notch width and the total size of the specimen is appreciably greater than zero. Finally, recall that in the second test the propagating crack reaches the central hole non-orthogonally. As the aim is to resolve the intersection of the propagating crack with the central hole, the regularization length introduced by the phase-field approach should be clearly smaller than the diameter of the hole. In a damage gradient approach, the crack would intersect the central hole (as well as any other boundary resolved by the regularization length) orthogonally (see, e.g., [82–87]).

## 5. Concluding remarks

### 5.1. Work done

In this work, quasistatic brittle fracture of a strain gradient elastic continuum has been modelled and numerically simulated using the finite-element method through utilization of the FEniCS library. The displacement field and the damage field were considered as the independent variables of the problem. Several energy functionals were defined. First, a deformation energy was defined depending on strain, strain gradient and damage fields. The involved effective stiffness coefficients were assumed to depend on damage. Second, the energy dissipated by damage was taken into account through a dissipative term depending on the damage field. Finally, the interaction with the external world was modelled using an external work term. Then, the solution of the weak form elasticity problem, for fixed damage, and of the Karush–Kuhn–Tucker conditions, obtained as a result of the maximum energy-release rate principle, has been addressed, aimed at finding the evolution of the two independent variables. Set up in this way, the problem was solved using the alternate minimization algorithm. Every iteration had two steps. First, the displacement field at equilibrium was computed while the damage field of the previous iteration was retained. Second, the damage field was updated by applying the Karush–Kuhn–Tucker conditions. The displacement field was computed by means of a finite-element method mixed formulation, which was implemented numerically using the FEniCS library. Simulation results have then been presented for two test cases on notched samples.

### 5.2. Results

The main outcomes of this work are the implementation itself, which is to, the authors’ best knowledge, the first computational implementation by an open-source library of the strain gradient energy approach to phase-field brittle fracture, and the validation of results obtained in [4] using commercial software. Results obtained in the two test cases that were considered, addressing crack onset and propagation from an initial notch, hint at the fact that using strain gradient modelling has many advantages, as well as in terms of physical accuracy, over existing approaches, which do not include strain gradient effects:

- There is no instability when computing the stress, and the resulting fields vanish within the crack, while being large around its tip and very much smaller far from it.
- Crack onset can be resolved within the notches, i.e., cracks do not necessarily have to surround the notch tip to give realistic results, and cracks can depart from notch wedges.
- Cracks can intersect boundaries non-orthogonally.


Thanks to the highly customizable computational platform that has been developed, it is possible to envision for the future the following extensions of this work:

- Passing from a mixed formulation to a non-mixed one by, e.g., isogeometric analysis;
- Implementing tip-following adaptive meshing, aimed at increasing the computational efficiency;
- Addressing dynamic analyses for studying crack propagation velocity, crack branching, etc.;
- Addressing anisotropic damaging;
- Exploiting strain splits, aimed at being able to differentiate (local) damage occurring in extension from that occurring in compression, or damage occurring in dilation from that occurring in shearing;
- Addressing ductile fracture;
- Running three-dimensional analyses.


## Funding

The author(s) received no financial support for the research, authorship and/or publication of this article.

## ORCID iDs

E Barchiesi  <https://orcid.org/0000-0002-7296-0671>

H Yang  <https://orcid.org/0000-0003-2080-3452>

L Placidi  <https://orcid.org/0000-0002-1461-3997>

## Notes

1. Here,  $I$  may be represented by the identity matrix in the previously defined Cartesian basis.
2. Here  $\delta\mathcal{E}(u, \omega)(\delta u, \delta\omega)$  denotes the Gateaux derivative of  $\mathcal{E}$  at  $(u, \omega)$  along the direction  $(\delta u, \delta\omega)$ .
3. A single damage variable shall be considered, to better elucidate the question.

## References

- [1] Cuomo, M, Contrafatto, L, and Greco, L. A variational model based on isogeometric interpolation for the analysis of cracked bodies. *Int J Eng Sci* 2014; 80: 173–188.
- [2] Bourdin, B, Francfort, GA, and Marigo, J-J. The variational approach to fracture. *J Elast* 2008; 91: 5–148.
- [3] Pham, K, Marigo, J-J, and Maurini, C. The issues of the uniqueness and the stability of the homogeneous response in uniaxial tests with gradient damage models. *J Mech Phys Solids* 2011; 59(6): 1163–1190.
- [4] Placidi, L, and Barchiesi, E. Energy approach to brittle fracture in strain-gradient modelling. *Proc R Soc London, Ser A* 2018; 474(2210): 20170878.
- [5] Bilotta, A, Morassi, A, and Turco, E. The use of quasi-isospectral operators for damage detection in rods. *Meccanica* 2018; 53(1–2): 319–345.
- [6] Bilotta, A, Morassi, A, and Turco, E. Damage identification in longitudinally vibrating rods based on quasi-isospectral operators. In: *8th European Workshop on Structural Health Monitoring (EWSHM 2016)*, 2016.
- [7] Misra, A. Effect of asperity damage on shear behavior of single fracture. *Eng Fract Mech* 2002; 69(17): 1997–2014.
- [8] Volkov, IA, Igumnov, LA, dell’Isola, F et al. A continual model of a damaged medium used for analyzing fatigue life of polycrystalline structural alloys under thermal–mechanical loading. *Continuum Mech Thermodyn* 2020; 32(1): 229–245.
- [9] Nasedkina, A, Eremeyev, V, and Nasedkin, A. Finite element simulation of transient axisymmetric thermoelastic problems for heterogeneous media with physical nonlinearities and circular fractures. In: *IV European Conference on Computational Mechanics*, 2010.
- [10] Della Corte, A, Battista, A, dell’Isola, F et al. (2017). Modeling deformable bodies using discrete systems with centroid-based propagating interaction: fracture and crack evolution. In: dell’Isola, F et al. (eds.) *Mathematical modelling in solid mechanics (Advanced Structured Materials, vol. 69)*. Singapore: Springer, 59–88.
- [11] Contrafatto, L, and Cuomo, M. A framework of elastic–plastic damaging model for concrete under multiaxial stress states. *Int J Plast* 2006; 22(12): 2272–2300.
- [12] Cuomo, M, and Fagone, M. Model of anisotropic elastoplasticity in finite deformations allowing for the evolution of the symmetry group. *Nanomech Sci Technol* 2015; 6(2): 135–160.
- [13] Cuomo, M. Forms of the dissipation function for a class of viscoplastic models. *Math Mech Complex Syst* 2017; 5(3): 217–237.
- [14] Yang, Y, and Misra, A. Higher-order stress–strain theory for damage modeling implemented in an element-free Galerkin formulation. *Comput Model Eng Sci* 2010; 64(1): 1–36.
- [15] Misra, A, and Singh, V. Micromechanical model for viscoelastic materials undergoing damage. *Continuum Mech Thermodyn* 2013; 25(2–4): 343–358.

- [16] Misra, A, and Poorsolhjouy, P. Granular micromechanics model for damage and plasticity of cementitious materials based upon thermomechanics. *Math Mech Solids*. Epub ahead of print 24 March 2015. DOI: 10.1177/1081286515576821.
- [17] Chen, Q, and Wang, G. Computationally-efficient homogenization and localization of unidirectional piezoelectric composites with partially cracked interface. *Compos Struct* 2020; 232: 111452.
- [18] dell'Isola, F, Maier, G, Perego, U et al. *The complete works of Gabrio Piola: vol. I*. Cham: Springer, 2014.
- [19] dell'Isola, F, Andreaus, U, and Placidi, L. At the origins and in the vanguard of peridynamics, non-local and higher-gradient continuum mechanics: an underestimated and still topical contribution of Gabrio Piola. *Math Mech Solids* 2015; 20(8): 887–928.
- [20] dell'Isola, F, Della Corte, A, and Giorgio, I. Higher-gradient continua: the legacy of Piola, Mindlin, Sedov and Toupin and some future research perspectives. *Math Mech Solids* 2017; 22(4): 852–872.
- [21] Misra, A, and Singh, V. Thermomechanics-based nonlinear rate-dependent coupled damage-plasticity granular micromechanics model. *Continuum Mech Thermodyn* 2015; 27(4–5): 787–817.
- [22] Toupin, RA. Elastic materials with couple-stresses. *Arch Ration Mech Anal* 1962; 11(1): 385–414.
- [23] Mindlin, RD, and Tiersten, HF. Effects of couple-stresses in linear elasticity. *Arch Ration Mech Anal* 1962; 11(1): 415–448.
- [24] Eremeyev, VA, Lebedev, LP, and Altenbach, H. *Foundations of micropolar mechanics*. Berlin: Springer Science & Business Media, 2012.
- [25] Eremeyev, VA and Altenbach, H. Equilibrium of a second-gradient fluid and an elastic solid with surface stresses. *Meccanica* 2014; 49(11): 2635–2643.
- [26] Eremeyev, VA, and Pietraszkiewicz, W. Material symmetry group and constitutive equations of micropolar anisotropic elastic solids. *Math Mech Solids* 2016; 21(2): 210–221.
- [27] Eremeyev, VA, dell'Isola, F, Boutin, C et al. Linear pantographic sheets: existence and uniqueness of weak solutions. *J Elast* 2018; 132(2): 175–196.
- [28] Tu, W, and Chen, Q. Evolution of interfacial debonding of a unidirectional graphite/polyimide composite under off-axis loading. *Eng Fract Mech* 2020; 230: 106947.
- [29] Giorgio, I. Numerical identification procedure between a micro-Cauchy model and a macro-second gradient model for planar pantographic structures. *Z Angew Math Phys* 2016; 67(4): 95.
- [30] Placidi, L, Andreaus, U, and Giorgio, I. Identification of two-dimensional pantographic structures via a linear D4 orthotropic second gradient elastic model. *J Eng Math* 2017; 103(1007): 1–21.
- [31] Abali, BE, Müller, WH, and Eremeyev, VA. Strain gradient elasticity with geometric nonlinearities and its computational evaluation. *Mech Adv Mater Mod Process* 2015; 1(1): 4.
- [32] Placidi, L, Rosi, G, Giorgio, I et al. Reflection and transmission of plane waves at surfaces carrying material properties and embedded in second-gradient materials. *Math Mech Solids* 2014; 19(5): 555–578.
- [33] Rahali, Y, Giorgio, I, Ganghoffer, JF et al. Homogenization à la Piola produces second gradient continuum models for linear pantographic lattices. *Int J Eng Sci* 2015; 97: 148–172.
- [34] Andreaus, U, dell'Isola, F, Giorgio, I et al. Numerical simulations of classical problems in two-dimensional (non) linear second gradient elasticity. *Int J Eng Sci* 2016; 108: 34–50.
- [35] Yang, H, Abali, BE, Timofeev, D et al. Determination of metamaterial parameters by means of a homogenization approach based on asymptotic analysis. *Continuum Mech Thermodyn* 2020; 32: 1251–1270.
- [36] Contrafatto, L, Cuomo, M, and Gazzo, S. A concrete homogenisation technique at meso-scale level accounting for damaging behaviour of cement paste and aggregates. *Comput Struct* 2016; 173: 1–18.
- [37] Placidi, L, Barchiesi, E, and Misra, A. A strain gradient variational approach to damage: a comparison with damage gradient models and numerical results. *Math Mech Complex Syst* 2018; 6(2): 77–100.
- [38] Placidi, L, and El Dhaba, AR. Semi-inverse method à la Saint-Venant for two-dimensional linear isotropic homogeneous second-gradient elasticity. *Math Mech Solids* 2017; 22(5): 919–937.
- [39] Placidi, L, Misra, A, and Barchiesi, E. Two-dimensional strain gradient damage modeling: a variational approach. *Z Angew Math Phys* 2018; 69(3): 56.
- [40] Yang, Y, and Misra, A. Micromechanics based second gradient continuum theory for shear band modeling in cohesive granular materials following damage elasticity. *Int J Solids Struct* 2012; 49(18): 2500–2514.
- [41] Placidi, L, Barchiesi, E, Misra, A et al. Variational methods in continuum damage and fracture mechanics. In: Altenbach, H and Öchsner, A (eds.) *Encyclopedia of continuum mechanics*. Berlin: Springer-Verlag, 2020.
- [42] dell'Isola, F, Seppecher, P, Placidi, L et al. Least action and virtual work principles for the formulation of generalized continuum models. In: dell'Isola, F and Steigmann, D (eds.) *Discrete and continuum models for complex metamaterials*. Cambridge: Cambridge University Press, 2020, 327–394.
- [43] dell'Isola, F, and Placidi, L. Variational principles are a powerful tool also for formulating field theories. In: dell'Isola F, and Gavriluk S (eds.) *Variational models and methods in solid and fluid mechanics (CISM Courses and Lectures, vol. 535)*. Vienna: Springer, 2011, 1–15.
- [44] dell'Isola, F, Madeo, A, and Seppecher, P. Cauchy tetrahedron argument applied to higher contact interactions. *Arch Ration Mech Anal* 2016; 219(3): 1305–1341.
- [45] dell'Isola, F, Seppecher, P, and Corte, AD. The postulations à la d'Alembert and à la Cauchy for higher gradient continuum theories are equivalent: a review of existing results. *Proc R Soc London, Ser A* 2015; 471(2183): 20150415.

- [46] Abali, BE, Müller, WH, and dell'Isola, F. Theory and computation of higher gradient elasticity theories based on action principles. *Arch Appl Mech* 2017; 87: 1495–1510.
- [47] Spagnuolo, M, Franciosi, P, and dell'Isola, F. (2020). A Green operator-based elastic modeling for two-phase pantographic-inspired bi-continuous materials. *Int J Solids Struct* 2020; 188: 282–308.
- [48] dell'Isola, F, Lekszycki, T, Spagnuolo, M et al. Experimental methods in pantographic structures. In: dell'Isola, F and Steigmann, D (eds.) *Discrete and continuum models for complex metamaterials*. Cambridge: Cambridge University Press, 2020, 263.
- [49] dell'Isola, F, Turco, E, and Barchiesi, E. Lagrangian discrete models: applications to metamaterials. In: dell'Isola, F and Steigmann, D (eds.) *Discrete and continuum models for complex metamaterials*. Cambridge: Cambridge University Press, 2020, 197.
- [50] dell'Isola, F, Spagnuolo, M, Barchiesi, E et al. Pantographic metamaterial: a (not so) particular case. In: dell'Isola, F and Steigmann, D (eds.) *Discrete and continuum models for complex metamaterials*. Cambridge: Cambridge University Press, 2020, 103.
- [51] Placidi, L, dell'Isola, F, and Barchiesi, E. Heuristic homogenization of Euler and pantographic beams. In: Picu, C and Ganghoffer, JF (eds.) *Mechanics of fibrous materials and applications (CISM International Centre for Mechanical Sciences (Courses and Lectures)*, vol. 596). Cham: Springer, 2020, 123–125.
- [52] De Angelo, M, Spagnuolo, M, D'Annibale, F et al. The macroscopic behavior of pantographic sheets depends mainly on their microstructure: experimental evidence and qualitative analysis of damage in metallic specimens. *Continuum Mech Thermodyn* 2019; 31(4): 1181–1203.
- [53] Misra, A, Singh, V, and Darabi, MK. Asphalt pavement rutting simulated using granular micromechanics-based rate-dependent damage-plasticity model. *Int J Pavement Eng* 2019; 20(9): 1012–1025.
- [54] Misra, A, and Sarikaya, R. Computational analysis of tensile damage and failure of mineralized tissue assisted with experimental observations. *Proc Inst Mech Eng H* 2020; 234(3): 289–298.
- [55] Placidi, L, Misra, A, and Barchiesi, E. Simulation results for damage with evolving microstructure and growing strain gradient moduli. *Continuum Mech Thermodyn* 2019; 31(4): 1143–1163.
- [56] Khakalo, S, and Niiranen, J. Anisotropic strain gradient thermoelasticity for cellular structures: plate models, homogenization and isogeometric analysis. *J Mech Phys Solids* 2020; 134: 103728.
- [57] Khakalo, S, and Niiranen, J. Lattice structures as thermoelastic strain gradient metamaterials: evidence from full-field simulations and applications to functionally step-wise-graded beams. *Composites, Part B* 2019; 177: 107224.
- [58] Turco, E, Golaszewski, M, Cazzani, A et al. Large deformations induced in planar pantographic sheets by loads applied on fibers: experimental validation of a discrete Lagrangian model. *Mech Res Commun* 2016; 76: 51–56.
- [59] Cazzani, A, Malagù, M, and Turco, E. Isogeometric analysis: a powerful numerical tool for the elastic analysis of historical masonry arches. *Continuum Mech Thermodyn* 2016; 28(1–2): 139–156.
- [60] Grillanda, N, Chiozzi, A, Bondi, F et al. Numerical insights on the structural assessment of historical masonry stellar vaults: the case of Santa Maria del Monte in Cagliari. *Continuum Mech Thermodyn*. Epub ahead of print 4 March 2019. DOI: 10.1007/s00161-019-00752-8.
- [61] Cazzani, A, Stochino, F, and Turco, E. An analytical assessment of finite element and isogeometric analyses of the whole spectrum of Timoshenko beams. *Z Angew Math Mech* 2016; 96(10): 1220–1244.
- [62] Schulte, J, Dittmann, M, Eugster, SR et al. Isogeometric analysis of fiber reinforced composites using Kirchhoff–Love shell elements. *Comput Methods Appl Mech Eng* 2020; 362: 112845.
- [63] Barchiesi, E, dell'Isola, F, Hild, F et al. Two-dimensional continua capable of large elastic extension in two independent directions: asymptotic homogenization, numerical simulations and experimental evidence. *Mech Res Commun* 2020; 103: 103466.
- [64] Cazzani, A, Malagù, M, and Turco, E. Isogeometric analysis of plane-curved beams. *Math Mech Solids* 2016; 21(5): 562–577.
- [65] Cazzani, A, Malagù, M, Turco, E et al. Constitutive models for strongly curved beams in the frame of isogeometric analysis. *Math Mech Solids* 2016; 21(2): 182–209.
- [66] Contrafatto, L, Cuomo, M, and Fazio, F. An enriched finite element for crack opening and rebar slip in reinforced concrete members. *Int J Fract* 2012; 178: 33–50.
- [67] Cuomo, M, and Greco, L. Isogeometric analysis of space rods: considerations on stress locking. In: *European Congress on Computational Methods in Applied Sciences and Engineering (ECOCOMAS 2012)*, 2012.
- [68] Greco, L, and Cuomo, M. B-spline interpolation of Kirchhoff–Love space rods. *Comput Methods Appl Mech Eng* 2013; 256: 251–269.
- [69] Greco, L, and Cuomo, M. An implicit G1 multi patch B-spline interpolation for Kirchhoff–Love space rod. *Comput Methods Appl Mech Eng* 2014; 269: 173–197.
- [70] Turco, E, and Aristodemo, M. A three-dimensional B-spline boundary element. *Comput Methods Appl Mech Eng* 1998; 155(1–2): 119–128.
- [71] Placidi, L. A variational approach for a nonlinear 1-dimensional second gradient continuum damage model. *Continuum Mech Thermodyn* 2015; 27(4–5): 623.
- [72] Placidi, L. A variational approach for a nonlinear one-dimensional damage-elasto-plastic second-gradient continuum model. *Continuum Mech Thermodyn* 2016; 28(1–2): 119.
- [73] Placidi, L, Andreus, U, Della Corte, A et al. Gedanken experiments for the determination of two-dimensional linear second gradient elasticity coefficients. *Z Angew Math Phys* 2015; 66(6) 3699–3725.



- [74] Phunpeng, V, and Baiz, P. Mixed finite element formulations for strain-gradient elasticity problems using the FEniCS environment. *Finite Elem Anal Des* 2015; 96: 23–40.
- [75] Zymbell, L, Mühlich, U, Kuna, M et al. A three-dimensional finite element for gradient elasticity based on a mixed-type formulation. *Comput Mater Sci* 2012; 52(1): 268–273.
- [76] Reiher, JC, Giorgio, I, and Bertram, A. Finite-element analysis of polyhedra under point and line forces in second-strain gradient elasticity. *J Eng Mech* 2017; 143(2): 04016112.
- [77] Scerrato, D, Zhurba Eremeeva, IA, Lekszycki, T et al. On the effect of shear stiffness on the plane deformation of linear second gradient pantographic sheets. *Z Angew Math Mech* 2016; 96(11): 1268–1279.
- [78] Erdogan, F, and Sih, GC. On the crack extension in plates under plane loading and transverse shear. *J Basic Eng* 1963; 85(4): 519–525.
- [79] Sih, GC. *Handbook of stress-intensity factors: stress-intensity factor solutions and formulas for reference*. Bethlehem, PA: Lehigh University, 1973.
- [80] Alibert, J-J, Seppecher, P, and Dell’Isola, F. Truss modular beams with deformation energy depending on higher displacement gradients. *Math Mech Solids* 2003; 8(1): 51–73.
- [81] dell’Isola, F, and Seppecher, P. Edge contact forces and quasi-balanced power. *Meccanica* 1997; 32(1): 33–52.
- [82] Miehe, C, Schaezel, L-M, and Ulmer, H. Phase field modeling of fracture in multi-physics problems. Part I. Balance of crack surface and failure criteria for brittle crack propagation in thermo-elastic solids. *Comput Methods Appl Mech Eng* 2015; 294: 449–485.
- [83] Nagaraja, S, Elhaddad, M, Ambati, M et al. Phase-field modeling of brittle fracture with multi-level *hp*-FEM and the finite cell method. *Comput Mech* 2019; 6: 1283–1300.
- [84] Miehe, C, Hofacker, M, and Welschinger, F. A phase field model for rate-independent crack propagation: robust algorithmic implementation based on operator splits. *Comput Methods Appl Mech Eng* 2010; 199(45–48): 2765–2778.
- [85] Huynh, G, Zhuang, X, and Nguyen-Xuan, H. Implementation aspects of a phase-field approach for brittle fracture. *Front Struct Civ Eng* 2019; 13(2): 417–428.
- [86] Chakraborty, P, Sabharwall, P, and Carroll, MC. A phase-field approach to model multi-axial and microstructure dependent fracture in nuclear grade graphite. *J Nucl Mater* 2016; 475: 200–208.
- [87] Hentati, H, Dhahri, M, and Dammak, F. A phase-field model of quasistatic and dynamic brittle fracture using a staggered algorithm. *J Mech Mater Struct* 2016; 11(3): 309–327.